Article

Nanoparticle MALDI-TOF Mass Spectrometry without Fragmentation: $Au(SCHCHPh)_n$ and Mixed Monolayer $Au(SCHCHPh)_n(L)_m$

Amala Dass, Anthony Stevenson, George R. Dubay, Joseph B. Tracy, and Royce W. Murray

J. Am. Chem. Soc., **2008**, 130 (18), 5940-5946 • DOI: 10.1021/ja710323t • Publication Date (Web): 08 April 2008

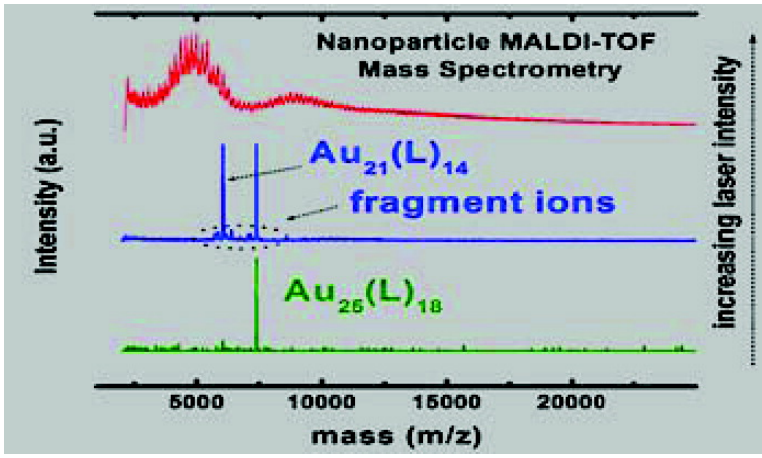

More About This Article

Additional resources and features associated with this article are available within the HTML version:

- Supporting Information
- Links to the 9 articles that cite this article, as of the time of this article download
- Access to high resolution figures
- Links to articles and content related to this article
- Copyright permission to reproduce figures and/or text from this article

View the Full Text HTML

J|A|C|S
ARTICLES

Published on Web 04/08/2008

Nanoparticle MALDI-TOF Mass Spectrometry without Fragmentation: $Au_{25}(SCH_2CH_2Ph)_{18}$ and Mixed Monolayer $Au_{25}(SCH_2CH_2Ph)_{18-x}(L)_x$

Amala Dass,[†] Anthony Stevenson,[†] George R. Dubay,[‡] Joseph B. Tracy,[†,§] and Royce W. Murray*[,†]

Kenan Laboratories of Chemistry, University of North Carolina, Chapel Hill, North Carolina 27599-3290, and Department of Chemistry, Duke University, Durham, North Carolina 27708

Received November 14, 2007; E-mail: rwm@email.unc.edu

Abstract: Intact molecular ions of the organothiolate-protected nanoparticle $Au_{25}(SCH_2CH_2Ph)_{18}$, including their isotopic resolution, can be observed at 7391 Da as 1− and 1+ ions in negative and positive mode, respectively, by MALDI-TOF mass spectrometry when using a tactic of threshold laser pulse intensities and *trans*-2-[3-(4-*tert*-butylphenyl)-2-methyl-2-propenylidene]malononitrile (DCTB) as matrix. Previous MALDI-TOF studies of Au nanoparticles using other matrices have encountered extensive fragmentation of nanoparticle as well as thiolate ligands. Absence of fragmentation enables precise determination of the distribution of mixed monolayer compositions on nanoparticles prepared by ligand exchange reactions and by synthesis using thiol mixtures. Reaction conditions producing mixed monolayers containing only one or a small number of usefully functional ligands can be readily identified. At increased laser pulse intensity, the first fragmentation step(s) for the $Au_{25}(SCH_2CH_2Ph)_{18}$ nanoparticle results in losses of AuL units and, in particular, loss of $Au_4(SCH_2CH_2Ph)_4$.

Introduction

The synthetic and analytical chemistry, catalytic, electronic, magnetic, and optical properties and reactivity of nanoparticles—especially their size-dependent properties—have generated and sustained substantial attention[1,2] since the early 1990s. The greatest interest has been in sizes near and below 5 nm. Nanoparticles that exhibit good stability are accessible by convenient synthetic pathways that offer manipulable flexibility in composition and, for which analytical tools have provided some defining compositional information, have been favored targets in this period of progress. Notable among them, for semiconductor and metal-based nanomaterials, respectively, are CdSe nanoparticles, which are often overcoated with Zn sulfide or (oxide) shells,[2f–h] and Au nanoparticles stabilized by attached thiolate monolayers[2d,e] (so-called monolayer-protected clusters, MPCs).

This report deals with the latter and, in particular, with a molecule-like nanoparticle MPC having the formula $Au_{25}(SCH_2CH_2Ph)_{18}$, as established by electrospray ionization mass spectrometry (ESI-MS),[3] including isotopically resolved[3b] results. The present work demonstrates that MALDI-TOF mass spectrometry can exert for this MPC a level of compositional definition and versatility similar to ESI-MS. By choice of a MALDI matrix reputed to assist ionization through electron transfer properties,[4] and by using a laser pulse intensity threshold approach, we have been able to suppress the extensive ligand and nanoparticle fragmentation typical in previous MALDI-TOF[5a–c] and laser desorption ionization (LDI)[5–7] observations, so as to detect intact $Au_{25}(SCH_2CH_2Ph)_{18}$ molecular ions.

[†] University of North Carolina.
[‡] Duke University.
[§] Present address: Department of Materials Science and Engineering, North Carolina State University, Raleigh, NC 27695.

(1) Whetten, R. L.; Khoury, J. T.; Alvarez, M. M.; Murthy, S.; Vezmar, I.; Wang, Z. L.; Stephens, P. W.; Cleveland, C. L.; Luedtke, W. D.; Landman, U. *Adv. Mater.* **1996**, *5*, 428–433.

(2) (a) Aiken, J. D., III; Finke, R. G. *J. Mol. Catal. A* **1999**, *145*, 1–44. (b) Love, J. C.; Estroff, L. A.; Kriebel, J. K.; Nuzzo, R. G.; Whitesides, G. M. *Chem. Rev.* **2005**, *105*, 1103–1169. (c) Daniel, M.-C.; Astruc, D. *Chem. Rev.* **2004**, *104*, 293–346. (d) Templeton, A. C.; Wuelfing, W. P.; Murray, R. W. *Acc. Chem. Res.* **2000**, *33*, 27–36. (e) Whetten, R. L.; Shafigullin, M. N.; Khoury, J. T.; Schaaff, T. G.; Vezmar, I.; Alvarez, M. M.; Wilkinson, A. *Acc. Chem. Res.* **1999**, *32*, 397–406. (f) Alivisatos, A. P. *Science* **1996**, *271*, 933–937. (g) Brus, L. E. *J. Phys. Chem.* **1986**, *90*, 2555–2560. (h) Murray, C. B.; Kagan, C. R.; Bawendi, M. G. *Science* **1995**, *270*, 1335–1338.

(3) (a) Tracy, J. B.; Kalyuzhny, G.; Crowe, M. C.; Balasubramanian, R.; Choi, J.-P.; Murray, R. W. *J. Am. Chem. Soc.* **2007**, *129*, 6706–6707. (b) Tracy, J. B.; Crowe, M. C.; Parker, J. F.; Hampe, O.; Fields-Zinna, C. A.; Dass, A.; Murray, R. W. *J. Am. Chem. Soc.* **2007**, *129*, 16209–16215.

(4) (a) McCarley, T. D.; McCarley, R. L.; Limbach, P. A. *Anal. Chem.* **1998**, *70*, 4376–4379. (b) Macha, S. F.; McCarley, T. D.; Limbach, P. A. *Anal. Chim. Acta* **1999**, *397*, 235–245.

(5) (a) Gutierrez, E.; Powell, R. D.; Furuya, F. R.; Hainfeld, J. F.; Schaaff, T. G.; Shafigullin, M. N.; Stephens, P. W.; Whetten, R. L. *Eur. Phys. J. D* **1999**, *9*, 647–651. (b) Schaaff, T. G.; Knight, G.; Shafigullin, M. N.; Borkman, R. F.; Whetten, R. L. *J. Phys. Chem. B* **1998**, *102*, 10643–10646. (c) Schaaff, T. G.; Whetten, R. L. *J. Phys. Chem. B* **2000**, *104*, 2630–2641. (d) Schaaff, T. G.; Shafigullin, M. N.; Khoury, J. T.; Vezmar, I.; Whetten, R. L.; Cullen, W. G.; First, P. N.; Gutierrez-Wing, C.; Ascensio, J.; Jose-Yacaman, M. J. *J. Phys. Chem. B* **1997**, *101*, 7885–7891. (e) Alvarez, M. M.; Khoury, J. T.; Schaaff, T. G.; Shafigullin, M.; Vezmar, I.; Whetten, R. L. *Chem. Phys. Lett.* **1997**, *266*, 91–98. (f) Schaaff, T. G.; Whetten, R. L. *J. Phys. Chem. B* **1999**, *103*, 9394–9396. (g) Schaaff, T. G.; Shafigullin, M. N.; Khoury, J. T.; Vezmar, I.; Whetten, R. L. *J. Phys. Chem. B* **2001**, *105*, 8785–8796.

10.1021/ja710323t CCC: $40.75

Achieving nonfragmenting (soft ionization) conditions makes it possible to analyze *mixtures* of nanoparticles having the same core atom count but with different mixed ligand shell compositions, such as the result from ligand exchange[8] reactions like

$$x\mathrm{R'SH} + \mathrm{Au_{25}(SCH_2CH_2Ph)_{18}} \rightarrow \mathrm{Au_{25}(SCH_2CH_2Ph)_{18-}}_x\mathrm{(SR')}_x + x\mathrm{HSCH_2CH_2Ph} \quad (1)$$

Exchange reactions are expected (as are nanoparticle syntheses from mixtures of thiol ligands) to produce mixtures of nanoparticles where x varies in (ideally) a Poisson fashion. The distribution arises from the statistical nature of reactions that (ideally) occur more or less independently at multiple potential reaction sites. The actual statistical nature of such ligand exchanges should of course respond in its details to variations among the rate constants of reactions at different core sites, effects of previous exchanges on nearby sites (such as by changes in steric environments), and to equilibrium constants of the exchange, among other factors. The $Au_{25}(SCH_2CH_2Ph)_{18}$ MPC consists of a Au_{13} core coated with six $-$SR$-$Au$-$SR$-$Au$-$SR$-$ semi-rings; there are two kinds of $-$SR ligand sites[9] on the semi-rings. While a ligand exchange kinetics study[10] showed a slowing in exchange kinetics after a few ligands were exchanged, this was a small effect (only ca. 20% in rate). To a first approximation, the $Au_{25}(SCH_2CH_2Ph)_{18}$ MPCs have $\sim$18 equally exchangeable sites.

Numerous reasons exist for seeking nanoparticles having mixed functionality in their ligand coating and for wanting to know the relative quantities of mixed functionalities. Imbalanced (average) exchanges[8a] and non-unity exchange equilibrium constants are known.[10] Studies[11] in which it is an important issue whether (or not) a nanoparticle's mixed monolayer composition equals the feed ratio of thiol (or other ligand) from which it was made would profit from the capacity to explicitly examine this problem. Actual measurements of mixed monolayer compositions have relied on methods yielding only *average* populations, such as FTIR[11c] and NMR.[12] Future exploitations of MPC properties that depend on knowing and ultimately controlling the population of specific functionalities on a nanoparticle, such as assembling geometrically targeted nanoassemblies, will rely on more explicit population assessments of functionalized linking sites. This paper shows the potential of assessing the numbers of such sites with MALDI mass spectrometry of $Au_{25}(SCH_2CH_2Ph)_{18-x}(SR')_x$ MPCs. Obtaining palpable quantities of MPCs within which x is invariant and determining the spatial distribution of sites over the nanoparticle core's surface is a further challenging goal that others[11] have approached in interesting ways.

Transmission electron microscopy (TEM) determination of nanoparticle physical size in the 1$-$2 nm diameter range is a generally unsatisfying experiment because its uncertainties can be larger than differences in diameters of nanoparticles having slightly differing atom count numbers.[13] This is particularly acute for Au MPCs with diameters $<$1.6 nm, the interesting regime in which molecule-like properties emerge.[13] High-resolution mass spectrometry and X-ray crystallography are more powerful research tools, and bringing them to bear has produced important recent progress for Au[3,9,14,15] and Pd nanoparticles.[16]

The early history of mass spectrometry of Au nanoparticles was dominated by laser desorption and MALDI-TOF experiments. Fackler et al.[17] applied ^{252}Cf plasma desorption mass spectrometry to a variety of Au nanoparticles including samples related to the case of $Au_{55}(PPh_3)_{12}Cl_6$. Interest in very small Au clusters based on more effective stabilizing organothiolate ligand shells grew following synthetic work by Brust et al.[18] and Whetten et al.[1,5c] and was promoted by the introduction of laser ionization desorption (LDI) mass spectrometry by Whetten et al.[1] In subsequent work, Whetten,[5] Reilly,[19] and Schaaff[20] applied LDI and MALDI-TOF mass spectrometry to the characterization of several MPCs, notably alkanethiolate and glutathionate-protected Au nanoparticles. The mass spectra showed extensive metal core and ligand fragmentation, especially in LDI,[5–7] and were burdened by consequent uncertainties in the determined masses of the parent nanoparticles. Nonetheless, identifying critical sizes at about 8, 14, 22, and 29 kDa[5d] provided crucial information to guide further synthesis and associations of MPC properties with their dimensions. Whetten[5b,c] and subsequently Tsukuda et al.[21] introduced electrospray ionization mass spectrometry in studies of very small glutathionate-protected Au clusters. None of these reports attained isotopic resolution of nanoparticle masses. The first high-

(6) (a) Balasubramanian, R.; Guo, R.; Mills, A. J.; Murray, R. W. *J. Am. Chem. Soc.* **2005**, *127*, 8126–8132. (b) Jimenez, V. L.; Georganopoulou, D. G.; White, R. J.; Harper, A. S.; Mills, A. J.; Lee, D.; Murray, R. W. *Langmuir* **2004**, *20*, 6864–6870.

(7) (a) Negishi, Y.; Tsukuda, T. *J. Am. Chem. Soc.* **2003**, *125*, 4046–4047. (b) Negishi, Y.; Tsukuda, T. *Chem. Phys. Lett.* **2004**, *383*, 161–165. (c) Tsunoyama, H.; Negishi, Y.; Tsukuda, T. *J. Am. Chem. Soc.* **2006**, *128*, 6036–6037. (d) Tsunoyama, H.; Nickut, P.; Negishi, Y.; Al-Shamery, K.; Matsumoto, Y.; Tsukuda, T. *J. Phys. Chem. C* **2007**, *111*, 4153–4158.

(8) (a) Ingram, R. S.; Hostetler, M. J.; Murray, R. W. *J. Am. Chem. Soc.* **1997**, *119*, 9175–9178. (b) Hostetler, M. J.; Templeton, A. C.; Murray, R. W. *Langmuir* **1999**, *15*, 3782–3789.

(9) Heaven, M. W.; Dass, A.; White, P. S.; Holt, K. M.; Murray,R. W. *J. Am. Chem. Soc.* **2008**, *130*, 3754–3755.

(10) Guo, R.; Song, Y.; Wang, G.; Murray, R. W. *J. Am. Chem. Soc.* **2005**, *127*, 2752–2757.

(11) (a) Jackson, A. M.; Myerson, J. W.; Stellacci, F. *Nat. Mater.* **2004**, *3*, 330–336. (b) Jackson, A. M.; Hu, Y.; Silva, P. J.; Stellacci, F. *J. Am. Chem. Soc.* **2006**, *128*, 11135–11149. (c) Centrone, A.; Hu, Y.; Jackson, A. M.; Zerbi, G.; Stellacci, F. *Small* **2007**, *3*, 814–817.

(12) (a) Warner, M. G.; Reed, S. M.; Hutchison, J. E. *Chem. Mater.* **2000**, *12*, 3316–3320. (b) Woehrle, G. H.; Brown, L. O.; Hutchison, J. E. *J. Am. Chem. Soc.* **2005**, *127*, 2172–2183. (c) Donkers, R. L.; Song, Y.; Murray, R. W. *Langmuir* **2004**, *20*, 4703–4707.

(13) (a) Woehrle, G. H.; Warner, M. G.; Hutchison, J. E. *J. Phys. Chem. B* **2002**, *106*, 9979–9981. (b) Woehrle, G. H.; Hutchison, J. E. *Inorg. Chem.* **2005**, *44*, 6149–6158. (c) Yang, Y.; Chen, S. *Nano Lett.* **2003**, *3*, 75–79. (d) Grant, C. D.; Schwartzberg, A. M.; Yang, Y.; Chen, S.; Zhang, J. Z. *Chem. Phys. Lett.* **2004**, *383*, 31–34. (e) Menard, L. D.; Gao, S.-P.; Xu, H.; Twesten, R. D.; Harper, A. S.; Song, Y.; Wang, G.; Douglas, A. D.; Yang, J. C.; Frenkel, A. I.; Nuzzo, R. G.; Murray, R. W. *J. Phys. Chem. B* **2006**, *110*, 12874–12883. (f) Menard, L. D.; Xu, H.; Gao, S.-P.; Twesten, R. D.; Harper, A. S.; Song, Y.; Wang, G.; Douglas, A. D.; Yang, Y. C.; Frenkel, A. I.; Murray, R. W.; Nuzzo, R. G. *J. Phys. Chem. B* **2006**, *110*, 14564–14573. (g) Bartlett, P. A.; Bauer, B.; Singer, S. J. *J. Am. Chem. Soc.* **1978**, *100*, 5085–5089. (h) Murray, R. W. *Chem. Rev.* **2008**, in press.

(14) Shichibu, Y.; Negishi, Y.; Watanabe, T.; Chaki, N. K.; Kawaguchi, H.; Tsukuda, T. *J. Phys. Chem. C* **2007**, *111*, 7845–7847.

(15) Jadzinsky, P. D.; Calero, G.; Ackerson, C. J.; Bushnell, D. A.; Kornberg, R. D. *Science* **2007**, *318*, 430–433.

(16) Mednikov, E. G.; Jewell, M. C.; Dahl, L. F. *J. Am. Chem. Soc.* **2007**, *129*, 11619–11630.

(17) McNeal, C. J.; Winpenny, R. E. P.; Hughes, J. M.; Macfarlane, R. D.; Pignolet, L. H.; Nelson, L. T. J.; Gardner, T. G.; Irgens, L. H.; Vigh, G.; Fackler, J. P., Jr. *Inorg. Chem.* **1993**, *32*, 5582–5590.

(18) Brust, M.; Walker, M.; Bethell, D.; Schiffrin, D. J.; Whyman, R. *J. Chem. Soc., Chem. Commun.* **1994**, 801–802.

(19) Arnold, R. J.; Reilly, J. P. *J. Am. Chem. Soc.* **1998**, *120*, 1528–1532.

(20) (a) Schaaff, T. G. *Anal. Chem.* **2004**, *76*, 6187–6196. (b) Schaaff, T. G. *Rapid Commun. Mass Spectrom.* **2003**, *17*, 2567–2570.

(21) Negishi, Y.; Nobusada, K.; Tsukuda, T. *J. Am. Chem. Soc.* **2005**, *127*, 5261–5270.

resolution electrospray results[3] became available for the specific case of the stable nanoparticle $Au_{25}(SCH_2CH_2Ph)_{18}$. Here, we expand high-resolution mass spectrometry of that nanoparticle and its mixed monolayer variants to the MALDI-TOF experiment.

We also note that the $Au_{25}(SCH_2CH_2Ph)_{18}$ MPC was earlier[10,22] mis-identified as having a composition $Au_{38}(SCH_2CH_2Ph)_{24}$. Published information on its electrochemistry,[22b] ligand exchange kinetics,[10] electron hopping dynamics,[22c] and NIR luminescence[22d] should be taken as referring to the $Au_{25}(SCH_2CH_2Ph)_{18}$ MPC described here.

Experimental Section

Chemicals. Sinapinic acid (SA), 4′-hydroxyazobenzene-2-carboxylic acid (HABA), "Universal Maldi Matrix", UMM (1:1 mixture of dihydroxybenzoic acid and α-cyano-4-hydroxycinnamic acid), *trans*-2-[3-(4-*tert*-butylphenyl)-2-methyl-2-propenylidene]-malononitrile (DCTB), acetonitrile (Fisher, >99.9%), methylene chloride (Fisher, 99.9%), methanol, hexanethiol (Fluka, >95%), and phenylethanethiol (Aldrich, 98%) were used as received. Methoxy pentaethylene glycol thiol (HS-PEG5) and methoxy ethylene glycol thiol (HS-PEG1) were synthesized as reported previously.[3,23] $Au_{25}(SCH_2CH_2Ph)_{18}$ and ligand-exchanged nanoparticles were prepared as reported previously.[3]

Mass Spectrometry. MALDI-TOF mass spectrometry experiments were performed using either an Applied Biosystems Voyager-DE Pro or Bruker Ultraflex I laser desorption linear or Reflectron time-of-flight mass spectrometer equipped with a nitrogen laser (337 nm). The accelerating voltage was held at 25 kV. Mass calibration was performed using protein standards (see Supporting Information).

MALDI Sample Preparation. The 1−100 mM matrix and analyte stock solutions were prepared as CH_2Cl_2 solutions and were mixed in microcentrifuge tubes at matrix/analyte ratios varying from 1:1 to 1000:1; 1–2 μL of this solution was applied to the sample plate and air-dried.

Results and Discussion

Gold clusters containing 25 atoms (Au_{25}) have been prepared previously (albeit initially mis-labeled as Au_{28}[5e] and as Au_{38}[10,22]). Numerous studies have characterized the properties of Au_{25} nanoparticles. Tsukuda[21] identified the Au_{25} atom count in experiments where a variety of kinetically arrested nanoparticles, stabilized by glutathionate ligands, were prepared and characterized by medium resolution ESI-MS. The $Au_{25}(glutathionate)_{18}$ nanoparticle was subsequently shown to exhibit strong stability,[21,24] including resistance to etching by thiols[25] which was attributed to geometric factors, that is, the completion of a cage structure around a core.[27a] $Au_{25}(glutathionate)_{18}$ clusters have also been prepared by ligand exchange of glutathione onto phosphine-stabilized Au_{11} clusters;[26] single-crystal X-ray structural analysis showed a biicosahedral structure for a $[Au_{25}(PPh_3)_{10}(SC_nH_{2n+1})_5Cl_2]^{2+}$ product.[14]

We will illustrate below that MALDI-TOF procedures that avoid nanoparticle ligand or core fragmentation are possible but under quite particular experimental conditions. MALDI-TOF mass spectrometry of the $Au_{25}(SCH_2CH_2Ph)_{18}$ nanoparticle using a DCTB matrix and high laser pulse power (similar to previously published MALDI protocols[5a–c]) produces spectra like that shown in Figure 1A. The broad peak centered at ~5 kDa corresponds to the Au_{25} core (4924 Da) from which ligands have been lost by S−C bond cleavage[19] and from which multiple and successive losses of Au and perhaps S atoms yield a "fine" structure with ca. 200–220 Da peak spacing. No obvious peak spacing feature identifiable as ligand loss (137 Da, the SCH_2CH_2Ph mass) is evident. Deducing the true molecular ion mass would require obviously difficult back-tracking on the trail of successively heavier nanoparticle fragments.

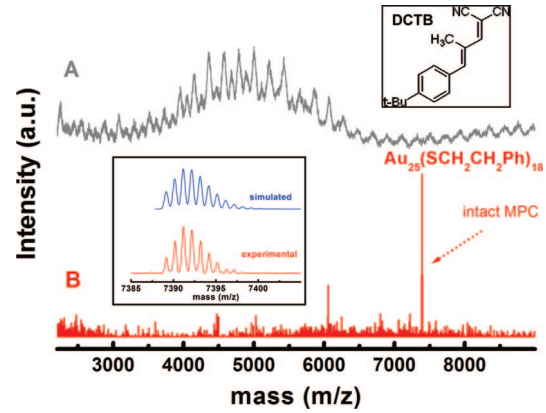

Figure 1. (A) Positive MALDI-TOF-MS spectrum (Applied Biosystems Voyager-DE Pro, in linear mode) of $Au_{25}(SCH_2CH_2Ph)_{18}$ with HABA matrix (gray). (B) Positive MALDI-TOF-MS spectrum (Bruker Ultraflex I in Reflectron mode) of $Au_{25}(SCH_2CH_2Ph)_{18}$ with DCTB matrix (red, see inset). Inset shows the expansion of isotopic resolution of the molecular ion peak. Blue spectrum is simulated, and red spectrum is the experimental data, shifted by 2 mass units.

Reilly showed[19] that nanoparticle fragmentation in laser desorption−ionization (LDI) is lessened at lowered laser intensities, but spectra of unfragmented nanoparticles remained elusive. We find, on the other hand, that MALDI-TOF in the DCTB matrix can at greatly reduced laser pulse power produce clean spectra (Figure 1, bottom curve) with a dominant peak at ~7391 Da. That particular nanoparticle mass has been firmly established by high-resolution electrospray mass spectrometry[3] as corresponding to the molecular ion of the $Au_{25}(SCH_2CH_2Ph)_{18}$ nanoparticle. The ligands in Figure 1B remain intact on the nanoparticle core at the lowered laser pulse intensity. The inset of Figure 1 shows a high-resolution MALDI spectrum of this region (taken in a reflectron mode), along with a simulated spectrum. There is a good match between the experimental and simulated isotopic distribution. There is also a 2 Da off-set between the experimental and simulated spectra that is ascribed to limitations in the spectrometer mass calibration, which was not done concurrently and further relied upon different matrices for spectra of the gold nanoparticle sample (DCTB) and the standards (HCCA and sinapinic acid). See Supporting Information for a description of the mass calibration procedure. We nonetheless point to the previous ESI-MS results as having established a known mass for the $Au_{25}(SCH_2CH_2Ph)_{18}$ nanoparticle, which could itself be regarded as an internal standard.

Note that Figure 1B shows a small fragment peak near 6 kDa with a mass of ~6060 Da that we assign to $Au_{21}(SCH_2CH_2Ph)_{14}$. This fragmentation is discussed later along with further details of the effects of laser pulse intensity and choice of matrix.

(22) (a) Donkers, R.; Lee, D.; Murray, R. W. *Langmuir* **2004**, *20*, 1945–1952. (b) Lee, D.; Donkers, R. L.; Wang, G.; Harper, A. S.; Murray, R. W. *J. Am. Chem. Soc.* **2004**, *126*, 6193–6199. (c) Choi, J.-P.; Murray, R. W. *J. Am. Chem. Soc.* **2006**, *128*, 10496–10502. (d) Wang, G.; Guo, R.; Kalyuzhny, G.; Choi, J.-P.; Murray, R. W. *J. Phys. Chem. B* **2006**, *110*, 20282–20289.
(23) Snow, A. W.; Foos, E. E. *Synthesis* **2003**, 509–512.
(24) Negishi, Y.; Chaki, N. K.; Shichibu, Y.; Whetten, R. L.; Tsukuda, T. *J. Am. Chem. Soc.* **2007**, *129*, 11322–11323.
(25) Shichibu, Y.; Negishi, Y.; Tsunoyama, H.; Kanehara, M.; Teranishi, T.; Tsukuda, T. *Small* **2007**, *3*, 835–839.
(26) Shichibu, Y.; Negishi, Y.; Tsukuda, T.; Teranishi, T. *J. Am. Chem. Soc.* **2005**, *127*, 13464–13465.

MALDI-TOF Analysis of Mixed Monolayers: $Au_{25}(SCH_2CH_2Ph)_{18-x}(L)_x$. As discussed above, many applications of nanoparticles may require their protecting or capping layers to contain one or more discretely identified functionalities. Au nanoparticles with mixed monolayers can be prepared by several routes, notably by Brust reaction[18] formation of the nanoparticle in the presence of multiple protecting ligands[8a] or by exchanges of the ligands on already formed nanoparticles with different ligands.[28] Ligand exchange (place exchange) reactions are versatile and have allowed preparation of ω-functionalized gold nanoparticles bearing electroactive, chromophore, ionophore, amino acid, spin labels, and metal–ligand groups.[8a] Ligand exchange dynamics in homogeneous[8b] and heterogeneous phase and substituent effects on ligand exchange[12] have been studied. Assessing the compositions of mixed monolayer Au MPCs requires methods differentially sensitive to monolayer components, which is possible using NMR[12,28] and FTIR[11c] spectroscopy. These methods yield, however, only *average* mixed monolayer compositions and thus do not display differences between individual nanoparticles in terms of proportions of their two (or more) monolayer ligand constituents. As discussed in the Introduction, the statistical nature of ligands binding to (or exchanging with) entities with multiple sites (the MPC resembles a many-ligand–metal complex) means that the nanoparticle products *will* be a mixture of different mixed monolayer compositions. In the context of nanoparticle populations produced in the Brust synthesis and in ligand exchange reactions, we refer to this as "ligand distributions". Apart from chromatographically separating nanoparticles with ligand distributions differing by only one ligand versus another—a feat not yet demonstrated—no method other than mass spectrometry can provide such information. It of course is necessary that the different ligands in the mixed monolayer have adequately different mass per ligand and, of course crucially, that spectra of unfragmented nanoparticles are accessible.

The middle spectrum in Figure 2 shows a MALDI-TOF mass spectrum of $Au_{25}(SCH_2CH_2Ph)_{18}$ at laser pulse intensities slightly more than the "threshold" that produce a small amount of fragmentation as seen by the peak at ~6060 Da. The top spectrum in Figure 2 corresponds to Au_{25} MPCs that had been subjected to a 22 h period of ligand exchange with a thiol (PEG5-SH; $CH_3(OCH_2CH_2)_5SH$) that is heavier by 130 Da than the original phenylethanethiolate ligand. Thus, a succession of peaks at higher mass appear (in the top spectrum), corresponding to differing numbers of PEG5-S- ligands that have replaced the SCH_2CH_2Ph ligands. Figure 2, bottom mass spectrum, shows an analogous result for a ligand exchange experiment using a thiol (PEG1-SH; $CH_3(OCH_2CH_2)SH$) that is lighter by 46 Da; again a series of mixed monolayer MPC masses result from differing numbers of the PEG1-S- ligand becoming incorporated into the MPC monolayer. The distribution of PEG5-S- thiolates on the Au_{25} MPCs in the Figure 2, top mass spectrum, shows peaks for molecular ions of as many as 12 nanoparticles that differ by the numbers of exchanged ligands. A smaller number of exchanged ligands, ~9, can be seen at the left, in the top spectrum for the Au_{21} fragment, roughly in line with the proportion of ligands (~four) lost from that fragment. This observation suggests that there is no strong preference for which kind of ligand became lost through fragmentation. The numbers of exchanged ligands can be assigned (in Figure 2, upper right) simply by counting from the original mass; the peak in the exchange series on the right that is labeled "7", for example, corresponds to the formula $Au_{25}(SCH_2CH_2Ph)_{11}(PEG5\text{-}S)_7$. Ligand exchange assignments were discussed in detail in our ESI-MS report on $Au_{25}(SCH_2CH_2Ph)_{18}$ nanoparticles.[3]

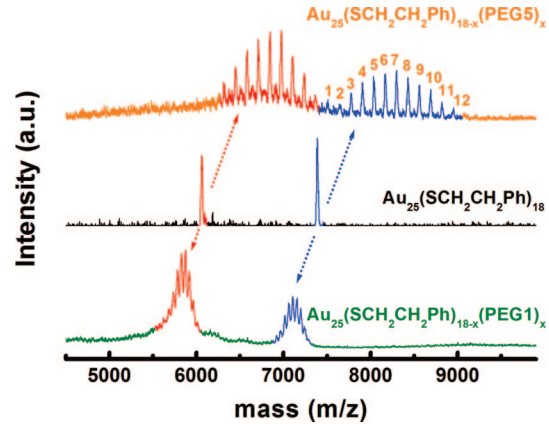

Figure 2. MALDI-TOF-MS spectra (Applied Biosystems Voyager-DE Pro) of $Au_{25}(SCH_2CH_2Ph)_{18}$ (middle curve) in positive linear mode and ligand exchange products (after 22 h) with PEG5-SH (top curve) and with PEG1-SH (bottom curve) in negative linear mode. In ligand exchanges, 1 mg of $Au_{25}(SCH_2CH_2Ph)_{18}$ was reacted with 100 mol excess of thiol in 200 μL of CH_2Cl_2 and was purified before analysis.

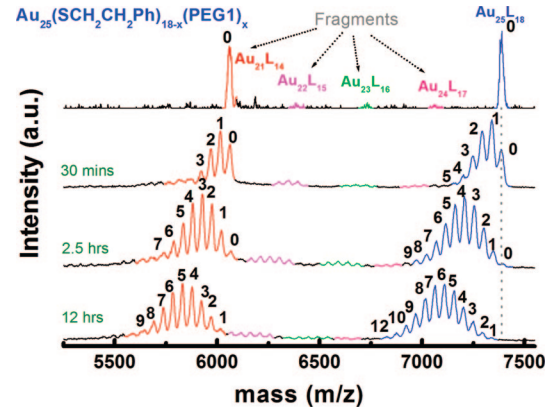

Figure 3. MALDI-TOF-MS spectra (Applied Biosystems Voyager-DE Pro) of $Au_{25}(SCH_2CH_2Ph)_{18}$ (top curve) in linear mode in DCTB matrix, showing ligand exchange products with PEG1-SH for zero time (top), 30 min, 90 min, and 12 h. The top spectrum was recorded in positive mode, and the bottom three spectra were recorded in negative mode. In ligand exchanges, 1 mg of $Au_{25}(SCH_2CH_2Ph)_{18}$ was reacted with 100 mol excess of thiol in 200 μL of CH_2Cl_2 and purified before analysis.

An extension of the above experiment is shown in Figure 3, where the MPC $Au_{25}(SCH_2CH_2Ph)_{18}$ is exchanged with the PEG1-SH thiol for differing periods of time. The spectral resolution in this experiment was substantially better than that in Figure 2, bottom; not only is the progress of the exchange reaction toward lower masses tracked but also the gradual increase in the specific number of different exchange products can be seen. The Au_{25} MPCs exchanged for 30 min show incorporation of up to ~5 PEG1-S- ligands, whereas exchange for 12 h results in incorporation of up to ~12 PEG1-S- ligands with undetectable amounts of unexchanged $Au_{25}(SCH_2CH_2Ph)_{18}$ MPCs remaining (no peak at lower right). The approximate symmetry of the distributions of exchange reaction products—

(27) (a) Ikeda, K.; Kobayashi, Y.; Negishi, Y.; Seto, M.; Iwasa, T.; Nobusada, K.; Tsukuda, T.; Kojima, N. *J. Am. Chem. Soc.* **2007**, *129*, 7230–7231. (b) Iwasa, T.; Nobusada, K. *J. Phys. Chem. C* **2007**, *111*, 45–49. (c) Iwasa, T.; Nobusada, K. *Chem. Phys. Lett.* **2007**, *441*, 268–272.

(28) Hostetler, M. J.; Green, S. J.; Stokes, J. J.; Murray, R. W. *J. Am. Chem. Soc.* **1996**, *118*, 4212–4213.

especially at longer times—is consonant with previous observations that the *average* (by NMR) exchange rate is roughly constant[10] over serial exchanges (i.e., a roughly uniform rate constant) for all available exchange sites on any given Au_{25} nanoparticle. It is worth pointing out that ligand exchange and ligand modification procedures have typically not considered the distribution issues shown by Figures 2 and 3.[29] As mentioned in the Introduction, the monolayer composition distributions in Figure 3 (12 h curve) should (ideally) follow a Poisson distribution; they do so (comparisons not shown) at least approximately in the current data. Further study is underway to elucidate the factors that underpin the observed distributions.

Figure 3 also helps to reveal some finer details of the fragmentation. Inspection of the small peaks in the mass interval between the Au_{21} and Au_{25} nanoparticles reveals low intensity "ripple" patterns that at longer exchange times systematically move to lower mass. These peaks are consistent with and are assigned to small quantities of $Au_{24}L_{17}$, $Au_{23}L_{16}$, and $Au_{22}L_{15}$ fragments that were not easily recognizable in the original (top) spectrum; that is, the pattern of ligand exchange was useful in recognizing small quantities of fragment ions. The presence of these fragments may be meaningful by reflecting that at least, in one fragmentation pathway, a *series* of Au_1L_l moieties can be lost in a sequence of reactions. As for the $Au_{21}L_{14}$ product, it is difficult to visualize a *one*-step loss of a Au_4L_4 unit from the $Au_{25}L_{18}$ nanoparticle, given its now-known[9] crystallographic content of −SR−Au−SR−Au−SR− semi-rings (which differs from a prior theoretical prediction[27]). However, possibly an intramolecular rearrangement/fragmentation might occur, driven by the special stability known[27a,30] for Au_4L_4 units or by an as-yet unknown special stability of a (gas-phase) $Au_{21}L_{14}$ composition. The availability of firm structural information[9] gives a first opportunity to speculate about the details of metal nanoparticle mass spectral fragmentation pathways.

Another ligand exchange experiment is illustrated in Figure 4, where $Au_{25}(SCH_2CH_2Ph)_{18}$ is reacted with hexanethiol (HSC6) for varying times. The ligand mass difference in this case is only 20 Da per ligand (lighter), and the average mass steadily moves to lower values as exchange proceeds. The putative limit of complete exchange is represented by a separately synthesized $Au_{25}(SC6)_{18}$ MPC, which gives a spectrum at the expected mass. Acquisition of the spectra in linear mode results in the broad nature of the $Au_{25}(SCH_2CH_2Ph)_{18}$ and $Au_{25}(SC6)_{18}$ MPCs. The exchange spectra again show that a wide distribution of mixed monolayer compositions is produced. The 12 h reaction product contains nanoparticles with from 3 to 12 new (-SC6) ligands. For such mixed monolayers, in general, the *average* number of ligands replaced can be measured by NMR,[8,12,31] but the result can be misleading because the properties and functional reactivities of the nanoparticles with different mixed monolayers can differ. Specifically, such variations pose a challenge for sophisticated assembly schemes that require each nanoparticle to have an identical monolayer composition. In this and Figures 2 and 3, it is also

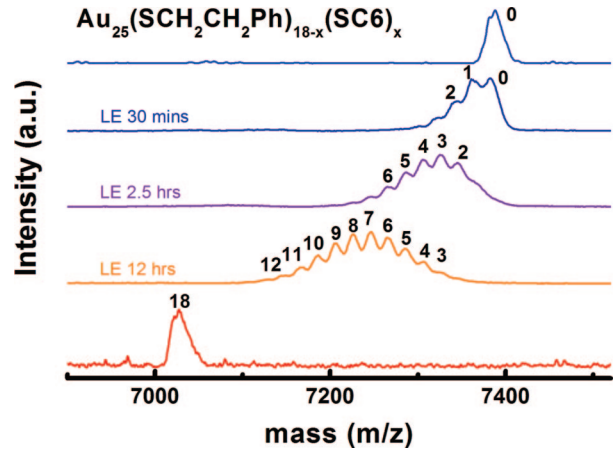

Figure 4. MALDI-TOF-MS spectra (Applied Biosystems Voyager-DE Pro) of $Au_{25}(SCH_2CH_2Ph)_{18}$ (top blue curve) in positive linear mode and (bottom curves) products of ligand exchanges with hexanethiol (C6SH) for 30 min, 150 min, and 12 h showing the distributions of the two ligands in the exchange products. The (bottom) red curve is that of separately synthesized $Au_{25}(SC6)_{18}$, for comparison purposes. In ligand exchanges, 1 mg of $Au_{25}(SCH_2CH_2Ph)_{18}$ was reacted with 100 mol excess of thiol in 200 μL of CH_2Cl_2 and purified before analysis.

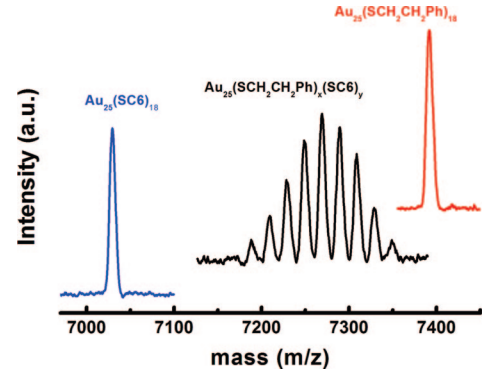

Figure 5. MALDI-TOF-MS spectra (Applied Biosystems Voyager-DE Pro) of $Au_{25}(SCH_2CH_2Ph)_{18}$ (red curve), $Au_{25}(SC6)_{18}$ (blue curve), and $Au_{25}(SCH_2CH_2Ph)_x(SC6)_y$ (black curve) in positive reflector mode. $Au_{25}(SCH_2CH_2Ph)_x(SC6)_y$ was prepared by Brust reaction using a mixture of 1:1 mol ratio of phenylethanethiol/hexanethiol in the nanoparticle Brust synthesis.

striking that the mixed monolayer ligand distribution is so *broad*. This probably reflects a lack of strong binding preferences among the particular ligands employed (as noted above), along with the large number of exchangeable ligands, and indeed is statistically expected.

Mixed monolayer MPCs can also be made by using mixtures of thiols in the initial nanoparticle synthesis. If the thiols are similar, the general expectation has been that the predominant Au core size produced is largely the same, and the monolayer composition reflects the reaction feed ratio of the different thiols. Figure 5 shows an example of preparing Au_{25} MPCs in this way, using the Brust reaction,[18] in a 1:1 mol ratio of phenylethane and hexane thiols—two structurally modestly dissimilar thiols. Wide distributions of mixed monolayer compositions are again produced; the distributions seen in Figures 2−4 are clearly not peculiar to the ligand exchange process and apply also to de novo synthesis. Importantly, the result of the 1:1 mol/mol thiol mixture synthesis reveals a mild preference in the product for the phenylethanethiolate ligand in the nanoparticle growth and passivation processes occurring during the Brust reaction. It has been commonly assumed in the use of this reaction that

(29) (a) Xu, X.; Rosi, N. L.; Wang, Y.; Huo, F.; Mirkin, C. A. *J. Am. Chem. Soc.* **2006**, *128*, 9286–9287. (b) Boal, A. K.; Ilhan, F.; DeRouchey, J. E.; Thurn-Albrecht, T.; Russell, T. P.; Rotello, V. M. *Nature* **2000**, *404*, 746–748. (c) Novak, J. P.; Feldheim, D. L. *J. Am. Chem. Soc.* **2000**, *122*, 3979–3980.
(30) (a) Gies, A. P.; Hercules, D. M.; Gerdon, A. E.; Cliffel, D. E. *J. Am. Chem. Soc.* **2007**, *129*, 1095–1104. (b) Gronbeck, H.; Walter, M.; Hakkinen, H. *J. Am. Chem. Soc.* **2006**, *128*, 10268–10275.
(31) Song, Y.; Huang, T.; Murray, R. W. *J. Am. Chem. Soc.* **2003**, *125*, 11694–11701.

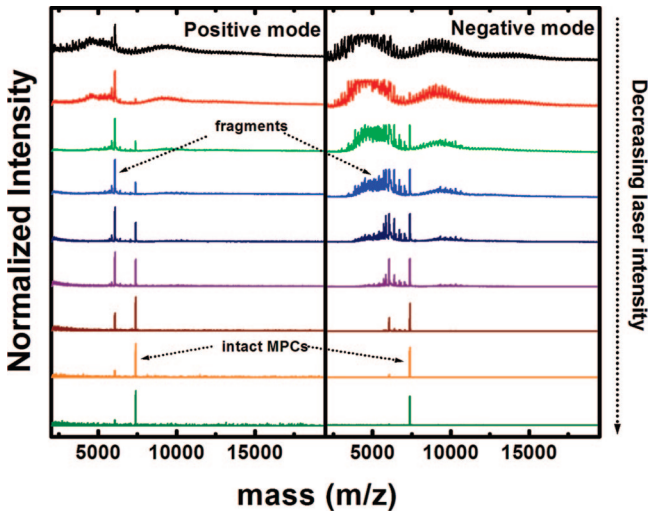

Figure 6. MALDI-TOF-MS spectra (Applied Biosystems Voyager-DE Pro) of $Au_{25}(SCH_2CH_2Ph)_{18}$ in DCTB matrix with varying laser intensity delineating the molecular ions from fragment ions in positive and negative linear mode. Some spectra here are clipped at the top; see Supporting Information for complete spectra examples.

the product nanoparticles bear the same proportion of ligands as the reaction feed ratio. There have been few openings into more detailed examination of the very complex nucleation/growth/passivation events in nanoparticle preparation. Analyses like that of Figure 5 may prove useful for further studies.

Intact Molecular Ions versus Fragment Ions. Preliminary MALDI-TOF experiments using the DCTB matrix gave spectra showing extensive fragmentation (like Figure 1, top), poorly reproducible relative intensities from sample to sample and in different spectral runs, and differences between positive and negative modes. Subsequent systematic variation of laser pulse intensity (in both positive and negative linear modes) gave results illustrated in Figure 6 (see Figure S-4 for some expanded images). High laser pulse intensities (top spectra) produced broad peaks at lowered mass (~5 kDa) corresponding to loss of ligands upon ionization and fragmenting of gold from the remnant cores. As the laser pulse intensity is greatly decreased (red and green curves), the broad fragment peak intensities diminish and two sharp peaks appear at ~6060 and ~7391 kDa. Further reductions in laser pulse intensity (blue, purple, brown, and orange) result in these sharp peaks becoming dominant in the spectrum. It is important to observe how the relative intensities of the latter two peaks change with decreasing laser pulse intensity; the ~6060 Da peak at first dominates, but then at lower laser intensity, it becomes less prominent and the ~7391 Da ion becomes the most intense ion present. The former is, thus, revealed as a fragmentation product of the latter. At the lowest intensity shown (green curve), the spectrum consists essentially entirely of the ~7391 ion, which as noted above is the expected molecular ion for the $Au_{25}(SCH_2CH_2Ph)_{18}$ nanoparticle. At even lower laser pulse intensities, the spectrum remains unchanged until becoming too weak to be observable above background noise.

Figure 6 demonstrates clearly that lowering the laser pulse intensity can lead to observation of a dominant molecular intact nanoparticle ion with minimal fragmentation, given a good choice of matrix. Unlike earlier studies that showed a variation of spectra between initial and subsequent laser pulses,[20a] we found that the spectra remain unchanged throughout the collection of up to 500 laser pulses.

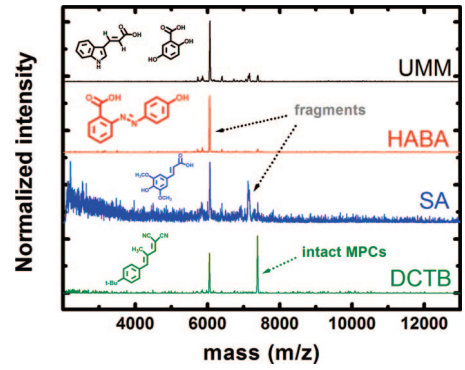

Figure 7. MALDI-TOF-MS spectra of (Applied Biosystems Voyager-DE Pro) $Au_{25}(SCH_2CH_2Ph)_{18}$ in UMM, HABA, SA, and DCTB matrix showing the superiority of DCTB matrix in obtaining molecular ion over fragment ions.

The above pattern of behavior was seen in both positive and negative mode MALDI-TOF mass spectrometry of $Au_{25}(SCH_2CH_2Ph)_{18}$, but there are significant differences between them. Negative mode spectra are more intense at equivalent laser power, and at threshold intensities, the residual amount of fragmentation was much less. It is possible that the higher intensity obtained in negative mode is due to the inherent 1− charge of the as-prepared Au MPCs.[3,9,24] At intermediate intensities, more fragmentation was observed in negative mode. Some of the fragments can be assigned to $Au_{24}(SCH_2CH_2Ph)_{17}$, $Au_{23}(SCH_2CH_2Ph)_{16}$, $Au_{22}(SCH_2CH_2Ph)_{15}$, and $Au_{21}(SCH_2CH_2Ph)_{14}$, again signifying a preferential loss of multiples of $Au_1(SCH_2CH_2Ph)_1$ from the intact nanoparticle molecular ion. At the highest intensities (topmost curves in Figure 6), the broadened spectra show "fine" structure peaks with regular spacing, ~197 Da, denoting Au atom losses from a ligand-denuded core. Additionally, at high laser pulse intensities, broad higher mass ions were observed at ~9 and ~13 kDa, which corresponded to larger core size nanoparticles formed in the Brust reaction synthesis[18] that were not completely removed during purification.

Choice of MALDI Matrix. Much of the success of this study can be attributed to a choice of MALDI matrix. Spectra of $Au_{25}(SCH_2CH_2Ph)_{18}$ using different matrices (in positive linear mode) show dramatically different results. Previous choices of nanoparticle matrices included sinapinic acid (SA), 4′-hydroxyazobenzene-2-carboxylic acid (HABA), and "Universal MALDI Matrix", UMM (1:1 mixture of dihydroxybenzoic acid and α-cyano-4-hydroxycinnamic acid), which are commonly used matrices in biological analysis and are thought to support *proton* transfer ionization. Figure 7 shows MALDI-TOF mass spectra of $Au_{25}(SCH_2CH_2Ph)_{18}$ in these matrices at lowered laser pulse intensity and in the *trans*-2-[3-(4-*tert*-butylphenyl)-2-methyl-2-propenylidene]malononitrile (DCTB) matrix used in previous figures. It is evident that mass spectra in the earlier matrices are dominated by fragment peaks; even at threshold laser intensities, none, *except DCTB*, show significant amounts of intact molecular ion.

The differences in the results in Figure 7 possibly originate from differing ionization mechanisms prevalent in the matrices illustrated. The matrices SA, UMM, and HABA are thought to promote proton transfer to the analyte or cation adduction.[4,32] In biological analyses, these matrices usually result in protonation and consequent cationization. Au nanoparticles with

(32) Knochenmuss, R. *Analyst* **2006**, *131*, 966–986.

nonpolar ligand shells (like $Au_{25}(SCH_2CH_2Ph)_{18}$) are, however, not proton acceptors and are not readily charged by protonation. As a consequence, previous MALDI matrices have produced spectra only when the laser pulse intensity was sufficient to evoke alternative ionization processes such as C−S bond cleavages.[19]

DCTB is reputed to promote electron transfer to/from the analyte.[33,34] It has been used for MALDI mass spectral observations of a variety of nonpolar, coordination, and organometallic compounds[35] and is reported to aid both positive and negative ionization at relatively low laser intensities (compared to other matrices).[33] Electron transfer in a MALDI matrix is feasible by ionization (or photoionization[4a]) of a matrix molecule that has a vertical ionization energy larger than that of the analyte.[4b] The experimental IE of DCTB is 8.54 eV,[36] which is comparable to reported theoretical values of 8.47[36] and 8.22 eV.[34] While calculated IE values of small gold clusters (up to 11 atoms) have been reported,[37] reliable values corresponding to that of 25 gold atoms are not available. If it is assumed that the DCTB matrix serves as an electron transfer agent, the IE of $Au_{25}(SCH_2CH_2Ph)_{18}$ must be lower than that of the matrix. The electrochemistry of $Au_{25}(SCH_2CH_2Ph)_{18}$ in its native form (now thought to be 1−) displays a one-electron oxidation step[22b] at a very mild potential of 85 mV versus Ag/AgCl, so the electron transfer matrix oxidation should be an efficient process.

An important virtue of an effective MALDI matrix is dominating photon absorbance so as to more gently dissipate the release of energy. The relative absorbances (A_{MPC}/A_{MATRIX}) of the Au_{25} nanoparticle and of the different matrices (at 337 nm) under a typical dilution condition (mole ratio 1:1000 MPC/matrix) are[38] 0.002, 0.004, 0.006, and 0.009 for matrices DCTB, SA, UMM, and HABA, respectively. These ratios show that indeed the DCTB matrix is a more efficient optical absorber compared to the others, but by a modest factor. A larger optical absorbance may thus to some degree add to the effectiveness of the DCTB as a nanoparticle MALDI matrix.

Acknowledgment. This research was supported by grants from the National Science Foundation and Office of Naval Research. We thank Dr. Viorel Mocanu and Dr. Carol Parker of the Duke−UNC Proteomics Facility for assistance with high-resolution MALDI-TOF measurements, Dr. Stephen Feldberg and Dr. Ramjee Balasubramanian for helpful discussions, and the reviewers for suggestion of discussion of optical absorbance efficiency.

Supporting Information Available: Au nanoparticle synthesis and detailed MALDI-MS figures. This material is available free of charge via the Internet at http://pubs.acs.org.

JA710323T

(33) Ulmer, L.; Mattay, J.; Torres-Garcia, H. G.; Luftmann, H. *Eur. J. Mass Spectrom.* **2000**, *6*, 49–52.
(34) Hoteling, A. J.; Nichols, W. F.; Giesen, D. J.; Lenhard, J. R.; Knochenmuss, R. *Eur. J. Mass Spectrom.* **2006**, *12*, 345–358.
(35) Wyatt, M. F.; Stein, B. K.; Brenton, A. G. *Anal. Chem.* **2006**, *78*, 199–206.
(36) Vasil'ev, Y. V.; Khvostenko, O. G.; Streletskii, A. V.; Boltalina, O. V.; Kotsiris, S. G.; Drewello, T. *J. Phys. Chem. A* **2006**, *110*, 5967–5972.
(37) Walker, A. V. *J. Chem. Phys.* **2005**, *122*, 1–12.
(38) These ratios are based on molar absorbance coefficients (337 nm) of 8.5×10^4, 4.1×10^4, 1.9×10^4, 1.5×10^4, and 0.9×10^4 for the nanoparticle and the four matrices, in order.